Chapter 4

Chapter 4: Plasmon-Phonon coupling and Energy-loss in Graphene Superlattice

We report our theoretical investigations on the Plasmon-phonon coupled modes, their interaction strength, damping and energy loss function in Graphene superlattice. The Superlattice is modeled to be repetition of SLG sheet in vertical z-direction, with dielectric medium embedded between the sheets. Our calculations are performed using RPA density-density response function of graphene. There exist both acoustic as well as optic coupled plasmon-phonon modes in superlattice. Analysis for strong coupling case for $qd<<1$ and for weak coupling case $qd>>1$, provides a linear dispersion i.e. $\omega(q) = q$ and q-independent frequency for wave vector tending to zero. Frequency of coupled modes is controlled by interlayer distance, d and charge density, n. In weak coupling limit (d is large) each layer behaves as an independent 2D Graphene sheet. On increasing n, magnitude of frequency reduces and coupling between layers becomes stronger. These coupled modes can attain frequency upto Mid-infrared (MIR) to Near Infrared (NIR) and also to visible light to an extent. Study of dispersion is useful for device application such as optoelectronic switches, photodetectors, modulators, image sensors, free-electron lasers. The mechanism of energy loss function can help in developing efficient energy storage devices based on Graphene superlattice.

4.1 Introduction

An interest has been sparked off in graphene based multilayer and superlattice structures because of their potential applications in technology and there have been extensive investigations, experimental as well as theoretical, on graphene superlattice and multilayer in recent past. Investigations have been done in past on

superlatiice structure by calculating wavevector-frequency dependent dielectric function, followed by study of collective excitations [1]. The collective excitation spectrum of a 2DEG gas interacting with LO phonon mode of host lattice is reported by Xiaoguang Wu and group. Their results include the analysis of intrasubband plasmons and the LO- phonon frequency, where a resonant coupling takes place and there is a splitting of Plasmon frequency. They have also evaluated the energy loss function and oscillator strength of Plasmon and phonon peaks for different values of the electron density [2**]** The coupled modes in semiconductor superlattice have helped in realizing many plasmonic devices. The modes can be experimentally detected by time-resolved visible pump and mid-infrared probe transmission spectroscopy [3]. Unique properties of graphene, inspired to think that graphene based multilayer and superlattice structures stand a better chance of application in device making industries. The interlayer interactions are strong enough to make it a better component that can be utilized in developing efficient electronic devices. There have been studies on transport and optical properties of graphene superlattice structure in recent years [4].

A superlattice structure is the stack of layers of two (or more) different materials arranged periodically one above another. The thickness between two consecutive layers ranges from micro to nanometers. These superlattice layers may have similar or different charge density and mass. This type of modified structures can be of great scientific and technological application, because of the enhancement in properties and work efficiency as compared to original crystal structures. Change in the properties can be attributed to the change in band structure of the superlattice. Plasmon that arises because of perturbation in Dielectric function of a system plays a major role in determining the optical properties of the material and hence it aids in

characterizing the material. Study of interaction of Plasmon with Phonon has opened new frontiers in Scientific and Industrial field [5,6].

Extensive investigations, both theoretical as well as experimental, have been carried out on the collective excitations in carbon nanotubes, 2DEG and various superlattice structures. Theoretical investigations on plasmons and the Plasmon-phonon coupled modes, energy loss function, damping rates, spectral weight have been reported for single layer gapless graphene (SLG) as well as for bilayer graphene (BLG) [7,8]. Coupled modes have been reported for SLG, bilayer and graphene based multilayers using generalized theory for massless Dirac particles [9]. Excitation spectrum and high-energy plasmons in SLG and in multilayer graphene systems [10,11], plasmonic excitations in Coulomb coupled N-layer balanced and unbalanced graphene structure was studied by J J Zhu et.al. at finite doping and temperatures [12], plasmon-phonon coupled modes in Graphene nanoribbon and graphene nanoribbons arrays have recently been investigated in view of applying graphene and graphene multilayer structures to plasmonic waveguides, modulators and detectors from sub-Tera hertz to mid-infrared regimes, and in obtaining efficient optoelectronic switching devices [13,14]. Plasmonic resonance in electrostatically gated graphene nanoribbons on SiO_2 has been recently studied by I.J.Luxmoore and group. They have reported of achieving frequency upto Far-Infrared regime [FIR] [15]. Role of phonons in understanding Plasmon dispersion has been studied in large-area Graphene dot and anti-dot arrays. The model has been considered as a suitable platform for light matter interactions and exploration of Plasmon-Phonon coupled modes. Their findings report an experimental attainable value of 20 meV of hybrid modes [16] HREELS experiment provides direct evidence of existencce of coupling of plasmons in sheet to in-plane optical phonons [17]. Excitation spectrum

in graphene have been studied by EELS for high incident energies (100keV) and at low incident energies (10 eV) by using HREELS [18]. Plasmons in Graphene reside in Terahertz to Mid-Infrared applications and hence it has emerged as a potential application in this frequency regime. Terahertz is tremendously high frequency range i.e. 0.3 to 3 THz while the Mid-Infrared regime has frequency range from 37-100 THz. An excellent review article has been written on Applications of Graphene Plasmonics in the working range of Terahertz to Mid-Infrared frequencies [19]. Xiaoguang Luo and group has also reported the applications of graphene plasmons in electronics, optics, energy storage, THz technology and so on [20].

CPPM can be studied with the help of Raman spectroscopy which incorporates scattering of light. This scattering is usually inelastic, where the kinetic energy of incident and scatttered light is different. Light scattering is an important physical phenomenon which contribute to the visible appearence of most objects, the other being absorption. Graphene superlattice can act as excellent light scatters as well. Raman scattering was studied in *n*-GaAs by S.Katayama and group. They reproduced the experimental results of spectra obtained by Raman Scattering from a coupled longitudinal optical (LO) phonon-damped mode, by taking into account the Landau damping of the mode itself as well as distribution of wave number of laser light due to the attenuation of light near the surface [21].

In this chapter we report our calculation for coupled Plasmon-phonon modes (CPPM), its interaction strength, damping and energy loss function, in Graphene based Superlattice (GBS). We have neglected the subband transition. Liu and Wills [22] have reported the coupled modes in epitaxial graphene, using angle-resolved reflection electron-energy-loss spectroscopy (AREELS). They have observed a transition from Plasmon like dispersion to phonon like dispersion when number of

graphene layers is increased on SiC substrate. We report plasmon-phonon coupled modes for GBS, where distance between two layers of Graphene is more than that of interatomic distance and graphene layers are equidistant with interlayer spacing being *d.*

Our modeled superlattice structures have been considered by various authors in past for obtaining electronic and optical properties. Few layer graphene encased between SiO_2 was proved as a promising structure in nano-scale thermal insulation [23]. The transfer matrix method has been implemented to obtain the transmittance, linear-regime conductance and electronic structure of Graphene Superlattice obtained by repeating alternate layers of Graphene with SiC/SiO_2 substrate [24]. Though, to best of our knowledge there has been no work reported on Plasmon-Phonon coupling of GBS.

The chapter is organized as follows: Formalism is presented in section 4.2. Section 4.3 reports the results and discussion and the references are quoted in section 4.4

4.2 Formalism

The calculations reported in this chapter have been performed within random phase approximation (RPA). The density-density response function has been calculated for a superlattice modeled to be an infinite periodic sequence of graphene layers in x-y plane embedded in dielectric medium of SiO_2 with a distance d between nearest graphene layers. Plasma oscillations of system are determined by computing zeros of dielectric function [25], while the imaginary part yields the damping rate of the modes.

$$\epsilon(q,\omega) = 1 - V(q)\chi(q,\omega) \tag{4.1}$$

V(q) is phonon screened electron-electron interaction, which is given by[26]

$$V(q) = \frac{2\pi e^2}{q\ \varepsilon(\omega)} S(q, q_z) \tag{4.2}$$

Where structure factor, $S(q, q_z)$ that depends on q and q_z, components of the wave vector parallel and perpendicular to the layers, is defined as,

$$S(q, q_z) = \frac{Sinh(qd)}{Cosh(qd) - Cos(q_z d)} \tag{4.3}$$

Dielectric function that incorporates the phonon modes of GBS is defined by,

$$\varepsilon(\omega) = \varepsilon_\infty \frac{\omega^2 - \omega_{LO}^2}{\omega^2 - \omega_{TO}^2} \tag{4.4}$$

ω_{LO} and ω_{TO} are the longitudinal optical and transverse optical phonon frequencies. ε_∞ is the optical dielectric constant. For computing our results, we used both full expressions as well as long wavelength limit expressions of polarization function. The long wavelength limit of $\chi(q, \omega)$ is given as [27]

$$\Pi(q, \omega) = \begin{cases} \frac{D_0 \gamma^2 q^2}{2\omega^2}\left[1 - \frac{\omega^2}{E_f^2}\right] for \ \ \gamma q < \omega < 2E_f \\ D_0 + \frac{i\omega}{\gamma q} \ \ when \ \ 0 < \omega < \gamma q \end{cases} \tag{4.5}$$

Where, $D_0 = 2k_F/\pi\gamma$ with $k_F = \sqrt{\pi n}$ is the Fermi wave vector. γ is band parameter and E_f is the Fermi energy.

The decay of coupled modes can be obtained by evaluating the equation [28]

$$\Gamma = \frac{Im(\epsilon(q, \omega))}{\frac{\partial}{\partial\omega} Re(\epsilon(q, \omega))\Big|_{\omega=\omega_\pm(q)}} \tag{4.6}$$

Combining Eqn. (4.1-4.5) and introducing $\omega \to \omega + i\eta$, where η is the damping term, we can easily obtain Real and imaginary parts of $\epsilon(q,\omega)$, by using Kramer-Kronigs relation for higher frequency regime. The Kramer-Kronig relation is given as [29]

$$\epsilon_1(q,\omega) = \frac{2}{\pi} P \int_0^\infty \frac{\omega' \epsilon_2(q,\omega')}{\omega'^2 - \omega^2} d\omega' \tag{4.7}$$

$$\epsilon_2(q,\omega) = -\frac{2\omega}{\pi} P \int_0^\infty \frac{\epsilon_1(q,\omega')}{\omega'^2 - \omega^2} d\omega' \tag{4.8}$$

4.3 Results and discussion

4.3.1 Plasmon-Phonon coupling and their damping

Coupled intraband as well as interband plasmon-phonon modes for GBS are given by zeros of Eq. (4.1). Energies of CPPM are function of q and q_z. q_z takes discrete values confined to $0 \le q_z \le \pi/d$. To compute results, we have used $\omega_{TO} = 95.0meV, \omega_{LO} = 118.75meV$, $\varepsilon_\infty = 6.4$, $\varepsilon_0 = 10.0$ Computed results are displayed for two values of $d = 400$Å & 800Å and two values of $n = 10^{12}\text{cm}^{-2}$ & 10^{14}cm^{-2} [8]. The effect of repetitive structure on collective excitations is manifested through $S(q,q_z)$. To study the effect of coupling between graphene layers in GBS, we calculated CPPM using Eqs.(4.2) to (4.5) in Eq.(4.1). For very weak coupling case, $S(q,q_z)$ has values very close to 1 and hence CPPM of GBS are not very different from those observed in SLG. For strong coupling case ($qd \ll 1$), $S(q,q_z)$ can be expressed as;

$$S(q,q_z)=\frac{qd}{1+\frac{(qd)^2}{2}-\cos(q_z d)} \tag{4.9}$$

Since,$-1<\cos(q_z d)<1$, CPPM lie within the bands of frequencies. Dispersion relations that describe lower and upper boundaries correspond to $\cos(q_z d)=\mp 1$. When phonon contribution is ignored, lower boundary of plasmon band is described by Plasmon dispersion $\omega_{pl}=\omega_0 qd/\sqrt{2}$ for small q-values, where $\omega_0=\left(2e^2E_f/d\varepsilon_0\right)^{1/2}$, with $\varepsilon_0=\frac{\varepsilon_\infty\omega_{Lo}^2}{\omega_{To}^2}$. Static dielectric constant for $\cos(q_z d)=-1$ is given by$\varepsilon(q)=1+d(\omega_0/\gamma)^2$, which is q-independent. On the other hand, when $\cos(q_z d)=1$, $q\to 0$ values of plasma energies are given by $\omega_{pu}=\omega_o\sqrt{2}$, which is dispersion less and $\varepsilon(q)=1+(q_s/q)^2$, with $q_s=2\omega_0/\gamma$. We thus notice that the behavior of GBS changes from semi-metallic to metallic as we vary $\cos(q_z d)$ from $-1\ to\ 1$. Long wavelength values of CPPM are given by;

$$\omega_{\pm}(q)=\frac{\sqrt{\omega_{LO}^2+M+\omega_{TO}^2\pm\sqrt{-4\omega_{TO}^2M+(\omega_{LO}^2+M+\omega_{TO}^2)^2}}}{\sqrt{2}} \tag{4.10}$$

Where, $M=2\frac{e^2}{\varepsilon_\infty}E_f qS(q,q_z)$

Equation (4.10) describes two modes for each value of $\cos(q_z d)$, one of which is plasmon like while other is phonon like. For $\cos(\mathrm{q_z d})=-1$, one of the two energies corresponds to $\omega_0 qd/\sqrt{2}$, while other is close to ω_{Lo} for $q\to 0$. When $\cos(\mathrm{q_z d})=1$ and $q\to 0$, plasmon like mode approximately approaches to $\omega_o\sqrt{2}$ and phonon like mode is close to $\left(\omega_{TO}^2+(\frac{\omega_{LO}q}{q_s})^2\right)^{1/2}$. We find that Plasmon-Phonon coupling is stronger at higher electron densities. It is to be noted that CPPM observed in GBS are very different than the coupled plasmon-phonon

modes found in SLG. Optical bulk like modes that has frequency $\omega_o\sqrt{2}$ and acoustic modes like $\omega_0 qd/\sqrt{2}$ cannot be observed in SLG.

Behavior of Plasmon mode for SLG and GBS differs drastically. For small q values the plasmon mode in SLG follows a $\sqrt{q}$ behavior [27] whereas it exhibits a linear dependence for GBS. Introduction of a structure factor not only changes the q-dependence, magnitude of plasma frequency changes too. The change in magnitude of plasma frequency is governed by the coupling constant and spacing between two consecutive Graphene layers in GBS.

The structure factor that arises due to repetitive structure in GBS significantly influences the coupling of plasmons and phonons. The CPPM of GBS shows entirely changed behavior and magnitude as compared to the behavior of coupled modes of SLG, as shown in Fig. 4.1. The figure displays two bands of coupled oscillations. The upper band involves optic frequencies ω_+(high frequency) while the lower band corresponds to acoustic frequencies ω_-(lower frequency). The CPPM of GBS for $d = 400\text{Å}$ and $n = 10^{12}\text{cm}^{-2}$, which are plotted in Fig. 4.1, are found very different than those observed in semiconductor superlattices [1].

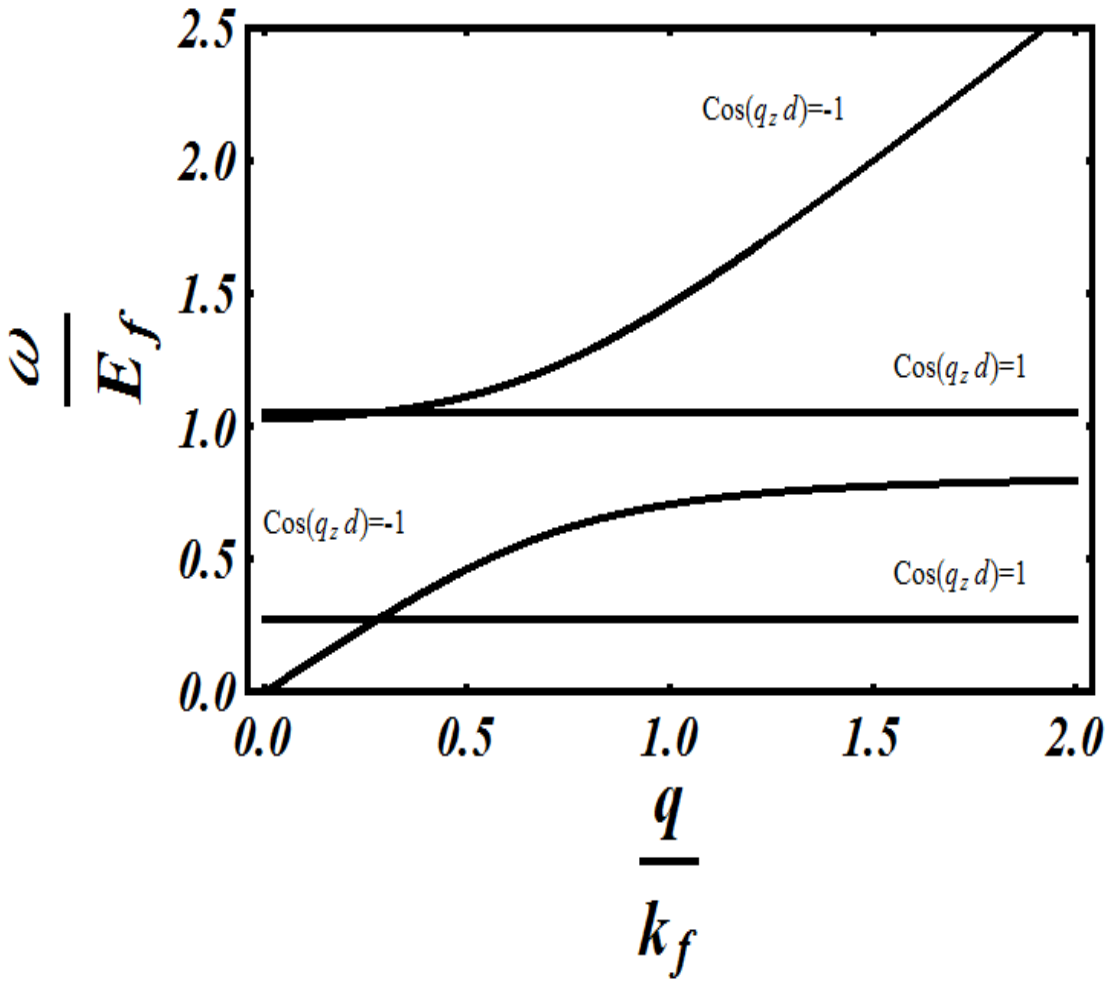

Figure 4.1 Plasmon-Phonon coupled modes for $n = 10^{12}\text{cm}^{-2}$ and $d = 400\text{Å}$

Fig 4.2 exhibits effect of change in *n* on CPPM in GBS. With increase in *n* the interaction becomes stronger and the bandwidth squeezes for a fixed value of *d* and the band accommodates itself within the band limits of acoustic mode occurring for the lower *n*- value, as can be seen from Figs. 4.2 and 4.3. The upper band that corresponds to high frequencies is narrower as compared with lower band which involves acoustic frequencies. Dispersion relations belonging to lower band follow linear dispersion for q upto $0.6k_f$. As the value of *n* is increased it enhances the plasmas in GBS, thereby increasing strength of Plasmon-phonon coupling.

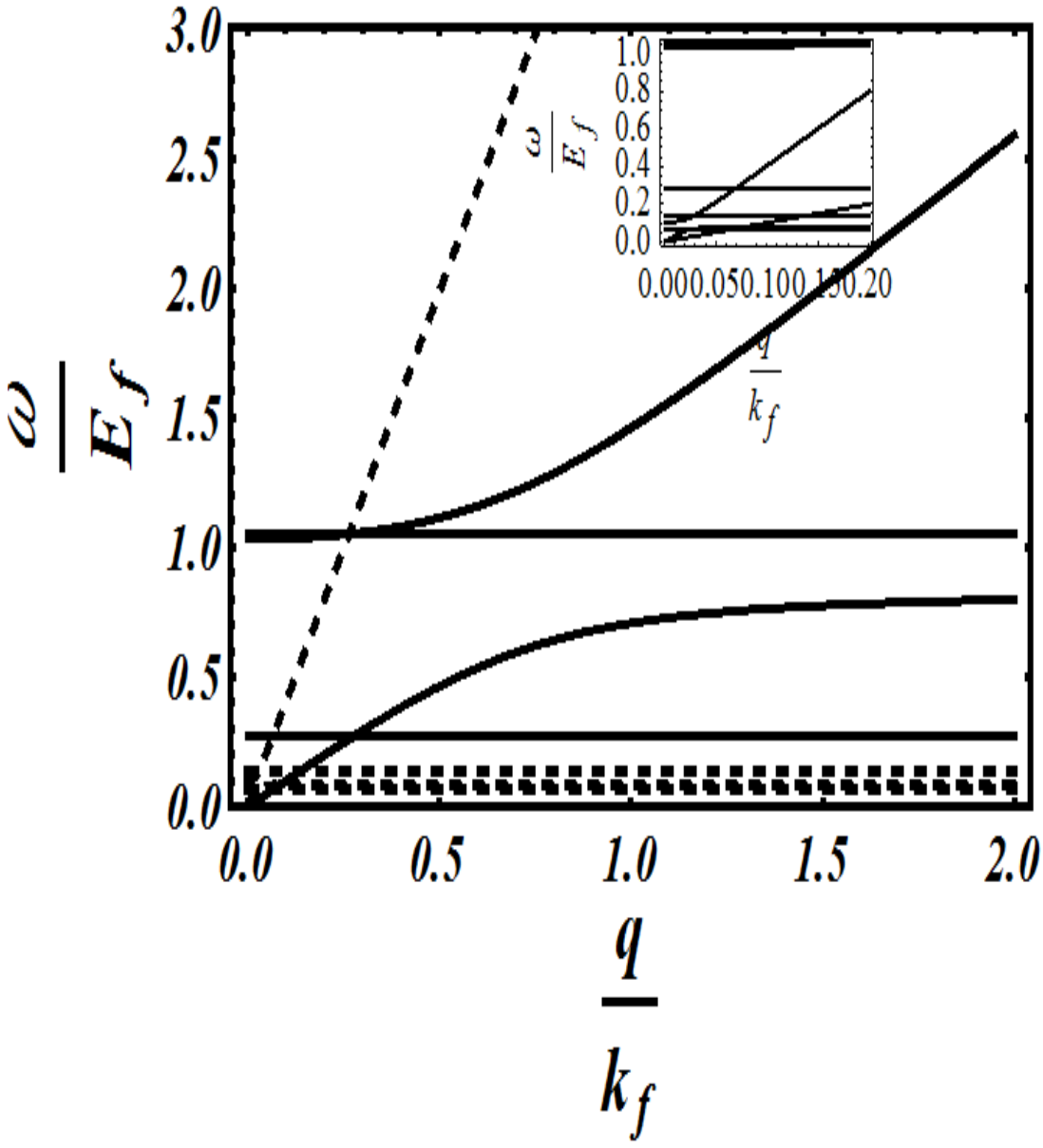

Figure 4.2 Analytical results of Plasmon-Phonon coupled modes, solid curve corresponds to $n = 10^{12} cm^{-2}$ while dotted line corresponds to $n = 10^{14} cm^{-2}$ for $d = 400$Å. Inset curves are upto $q < 0.2k_f$

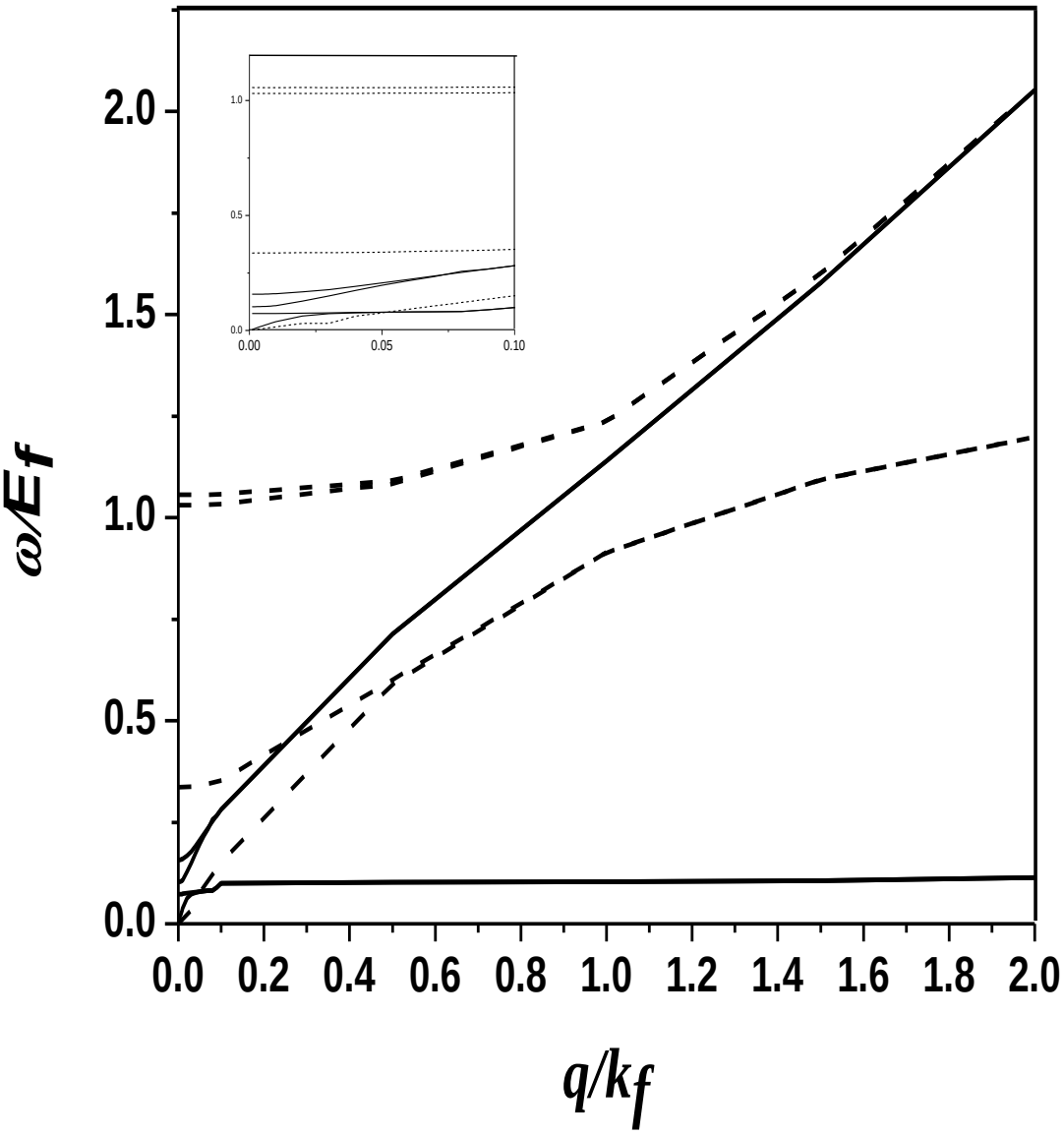

Figure 4.3 Plasmon-Phonon coupled modes obtained using full polarization for $d = 400\text{Å}\ n = 10^{12}cm^{-2}\ (dashed\ curve)\ \ n = 10^{14}cm^{-2}(solid\ curve)$. Inset shows coupled modes $q < 0.1k_f$

Fig 4.4 and 4.5 display the CPPM for two different values of *d* keeping *n* fixed. The figure shows two bands for the coupled oscillations. The upper band is narrower while the lower band is wider. With increase in the interlayer distance i.e.

from 400Å *to* 800Å, and keeping *n* constant, width of bands magnitude of frequency at a *q*-value, as shown in Fig 4.5.

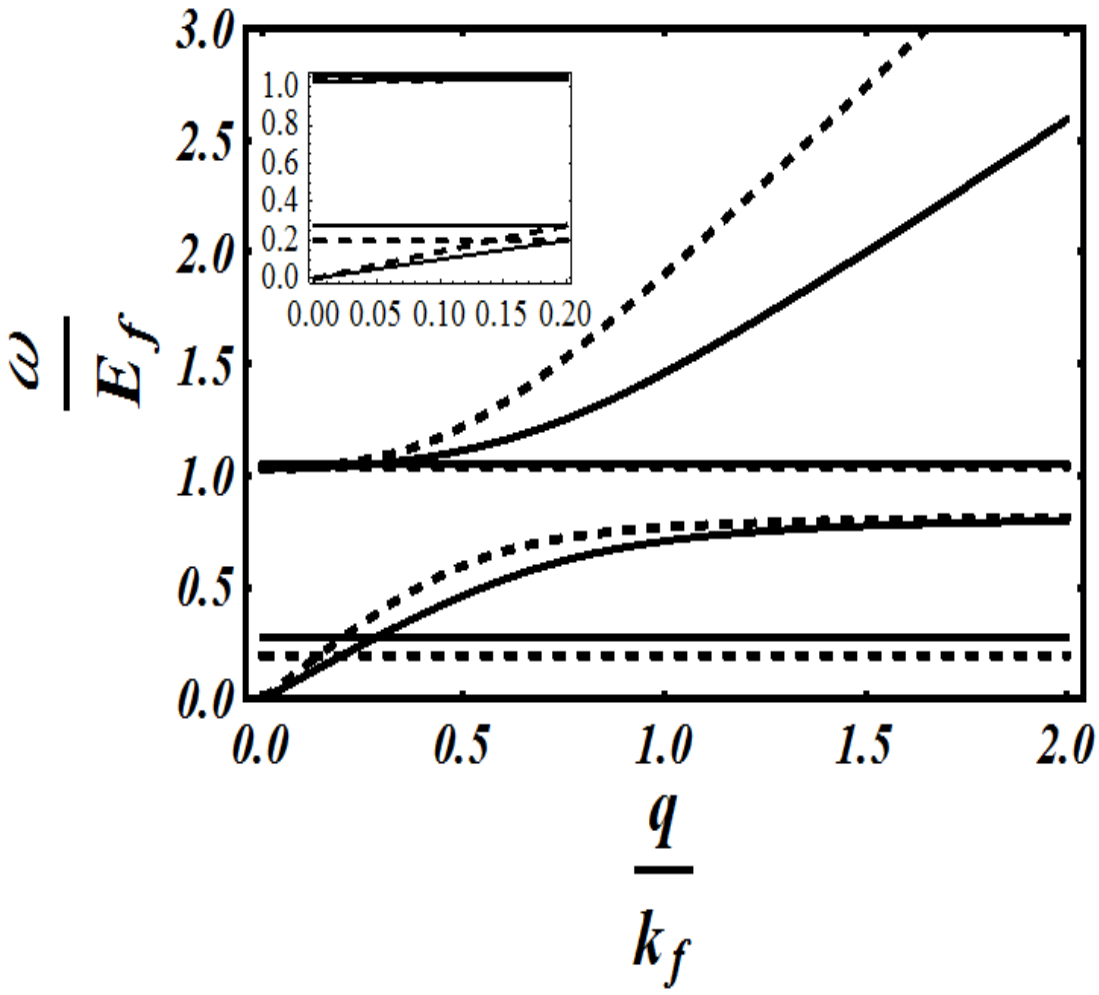

Figure 4.4 Plasmon-Phonon coupled modes for $d = 800Å$ (dashed curve) and $d = 400Å$ (solid curve) for $n = 10^{12}cm^{-2}$. Inset curves are upto $q < 0.2k_f$

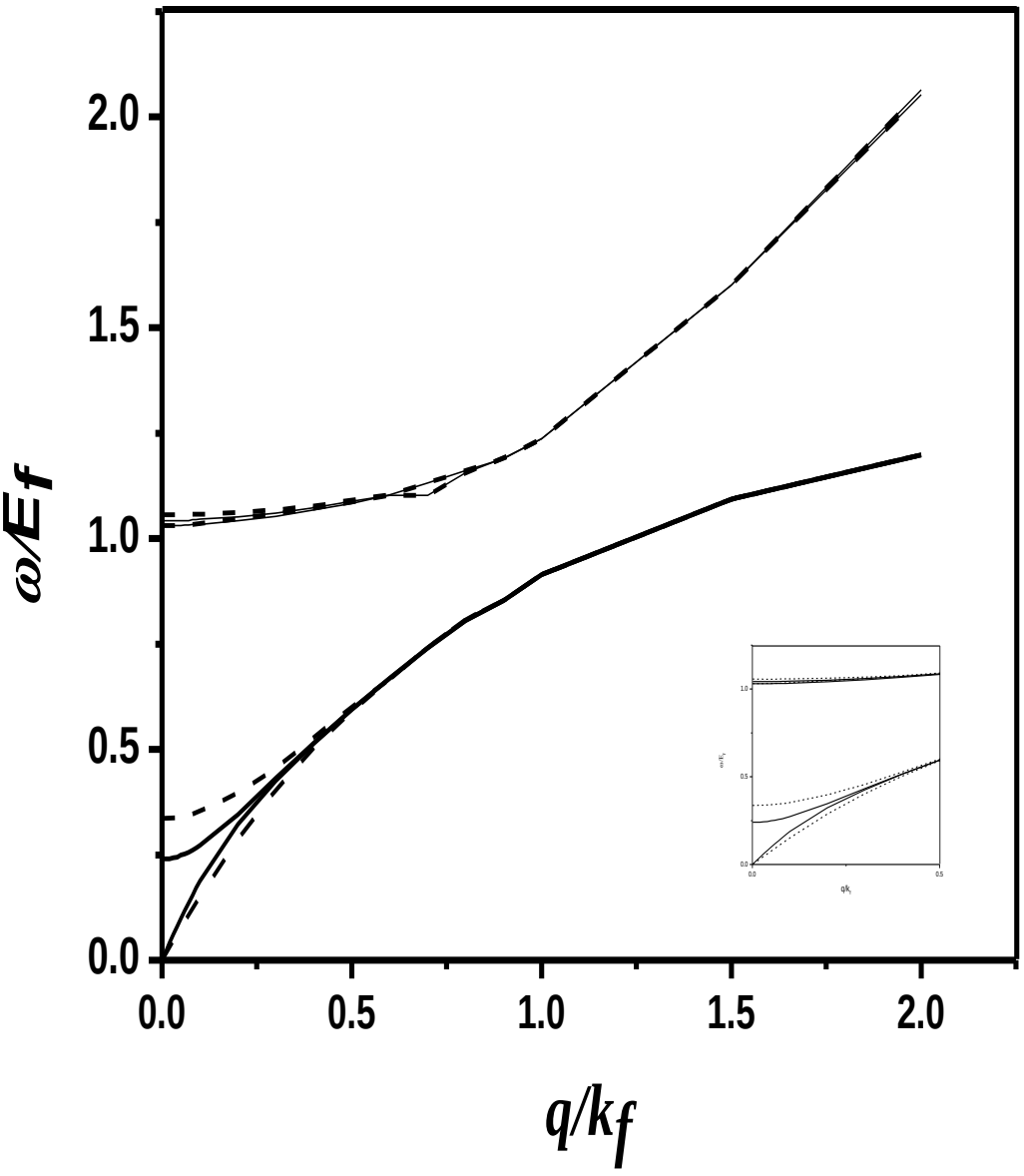

Figure 4.5 Numerical results for Plasmon-Phonon coupled modes, dashed curve corresponds to $d = 400$Å while solid line corresponds to $d = 800$Å for $= 10^{12} cm^{-2}$. Inset curves are upto $q < 0.5k_f$

Weak Coupling Case

Taking $qd \to \infty$ in equation (4.3) we obtain

$$\epsilon(q,\omega) = 1 - \frac{2\pi e^2}{q\,\varepsilon_\infty \frac{\omega^2-\omega_{LO}^2}{\omega^2-\omega_{TO}^2}}\,\Pi(q,\omega) \qquad (4.11)$$

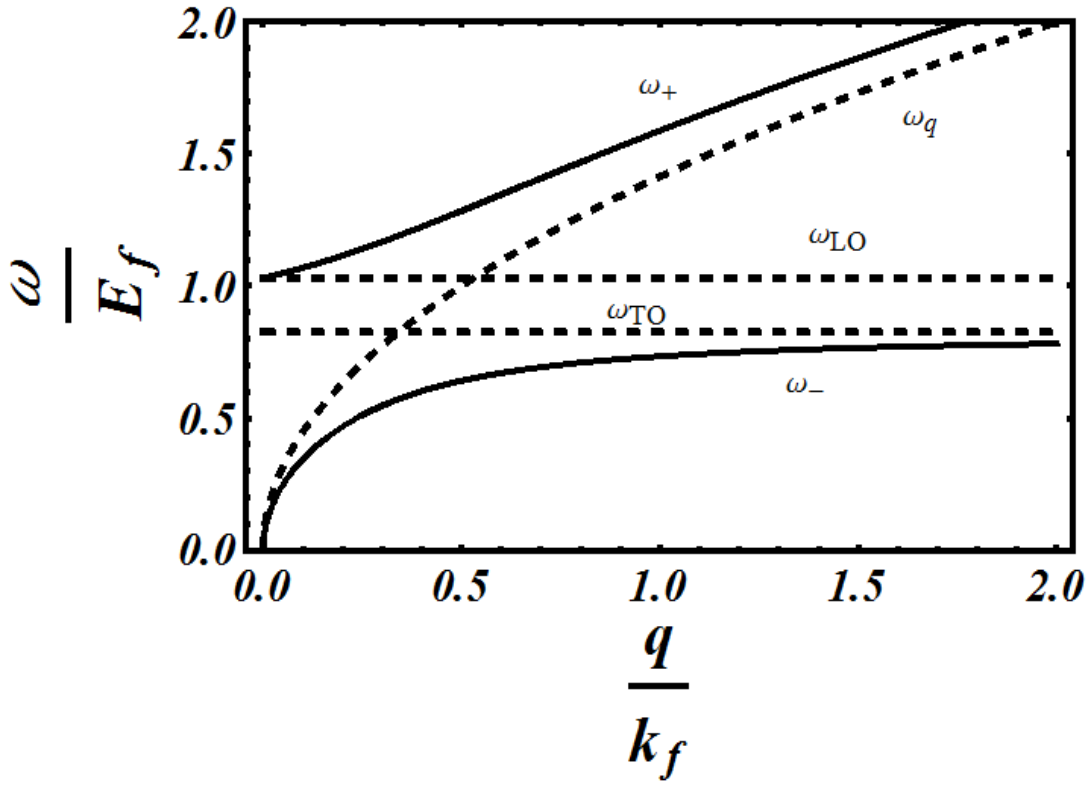

Figure 4.6 Plasmon-Phonon coupling mode for weak coupling. Dashed curves displays ω_+ and ω_- modes. Uncoupled modes are shown by ω_{LO}, ω_{TO} (Dotted curves), while solid curve displays plasmon mode ω_q without plasmon-phonon coupling.

Equation (4.6) is basic plasmon-phonon equation for a regular 2D graphene. In weak coupling limit each layer behaves as independent 2D Graphene sheet [8]. For Weak Coupling (Figure 4.6) depicts Plasmon-Phonon coupling i.e. ω_+ and ω_- (dashed curves). ω_{LO}, ω_{TO} and ω_q are the uncoupled modes. The uncoupled mode ω_{LO} is similar to ω_+ mode for small values of $\frac{q}{k_f}$, while ω_{TO} almost matches ω_- for larger values of $\frac{q}{k_f}$. The coupling strength ratio is in given as [30]

$$\frac{R_\pm}{R_0} = \frac{\omega_\pm \omega_{LO}(\omega_\pm{}^2 - \omega_{TO}{}^2)}{(\omega_\pm{}^2 - \omega_\mp{}^2)(\omega_{LO}{}^2 - \omega_{TO}{}^2)}$$

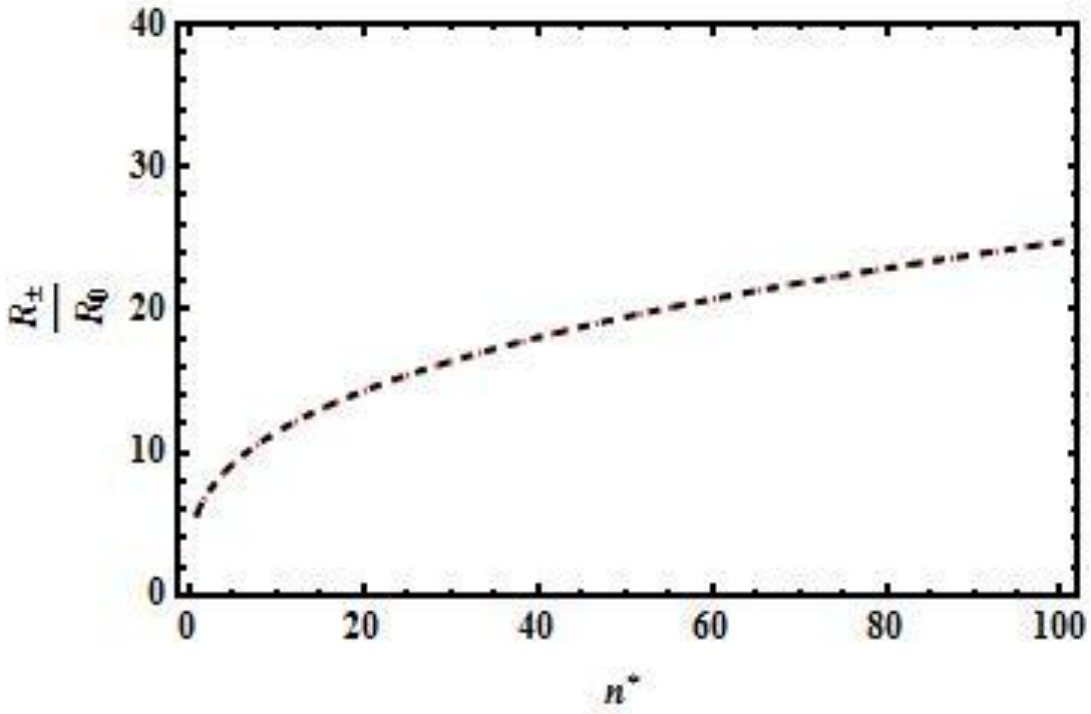

Figure 4.7 Coupling mode interaction strength ($\frac{R_\pm}{R_0}$) vs. *n* for GBS for $d = 800$Å.

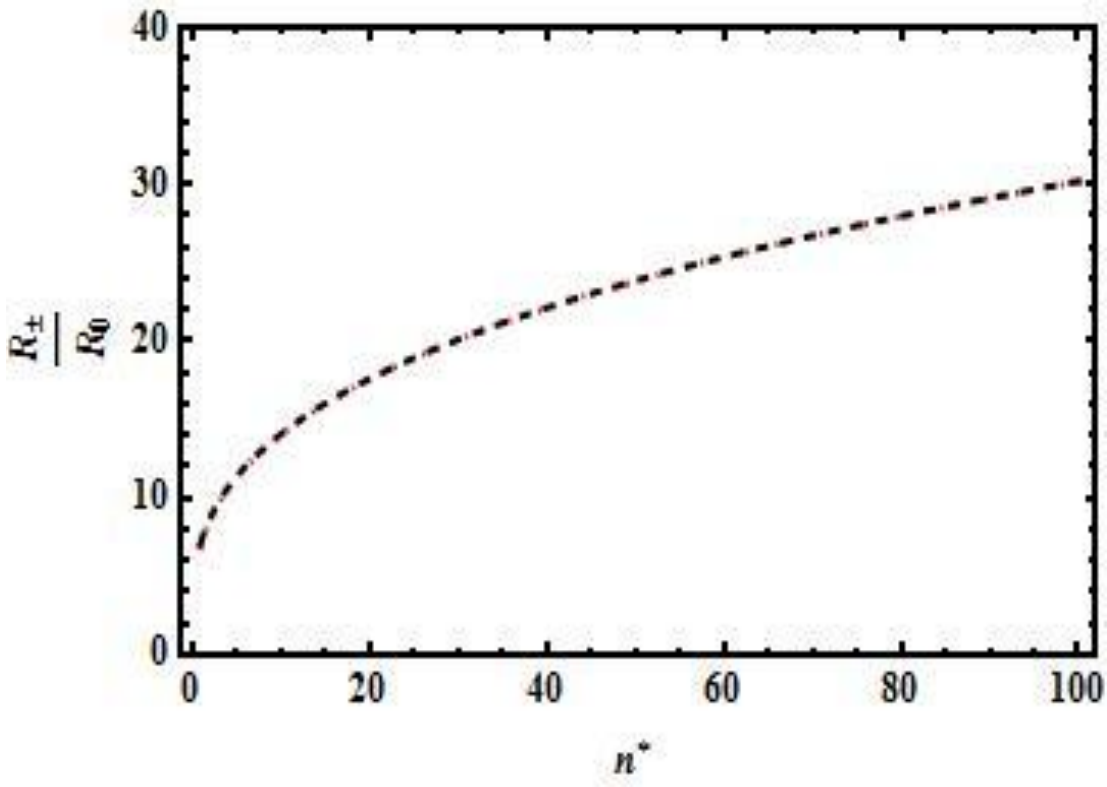

Figure 4.8 Coupling mode interaction strength ($\frac{R_\pm}{R_0}$) vs. *n* for GBS for $d = 400$Å.

The coupling of CPPM gets stronger as *d* decreases i.e. away from SLG limits, as can be seen from Figs 4.7 and 4.8. $\frac{R_{\pm}}{R_0}$ gives the ratio of coupling strength with respect to density *n* , where *n* is considered as $n = \sqrt{n^* \times 10^{12}}$ in this case.

The decay of coupled modes can be obtained using equ (4.8) we obtain the real and imaginary parts of ϵ within long wavelength limit for high frequency regime as,

$$\epsilon_2(q,\omega) = -i\pi L\delta(\omega^2 - {\omega_{LO}}^2) \tag{4.12}$$

$$\epsilon_1(q,\omega) = 1 - \frac{L}{\omega^2 - {\omega_{LO}}^2} + \frac{L1}{\omega^2} \tag{4.13}$$

where, $L = \frac{2\pi e^2}{\varepsilon_0 q}\frac{{\omega_{LO}}^2}{{\omega_{TO}}^2} D_0 \frac{\gamma^2 q^2}{2}(\omega^2 - {\omega_{TO}}^2)(\frac{1}{{\omega_{LO}}^2} - \frac{1}{4E_f^2})$

and, $L1 = \frac{L}{(\frac{1}{{\omega_{LO}}^2} - \frac{1}{4E_f^2})}$

While, for low frequency region the real and imaginary parts can be directly obtained using equation (4.1-4.5). The energy loss during damping process is discussed in next section.

The damping in low frequency regime has been evaluated. There is no significant change in damping when d is changed while damping in this regime changes drastically when *n* is changed as shown in figures below.

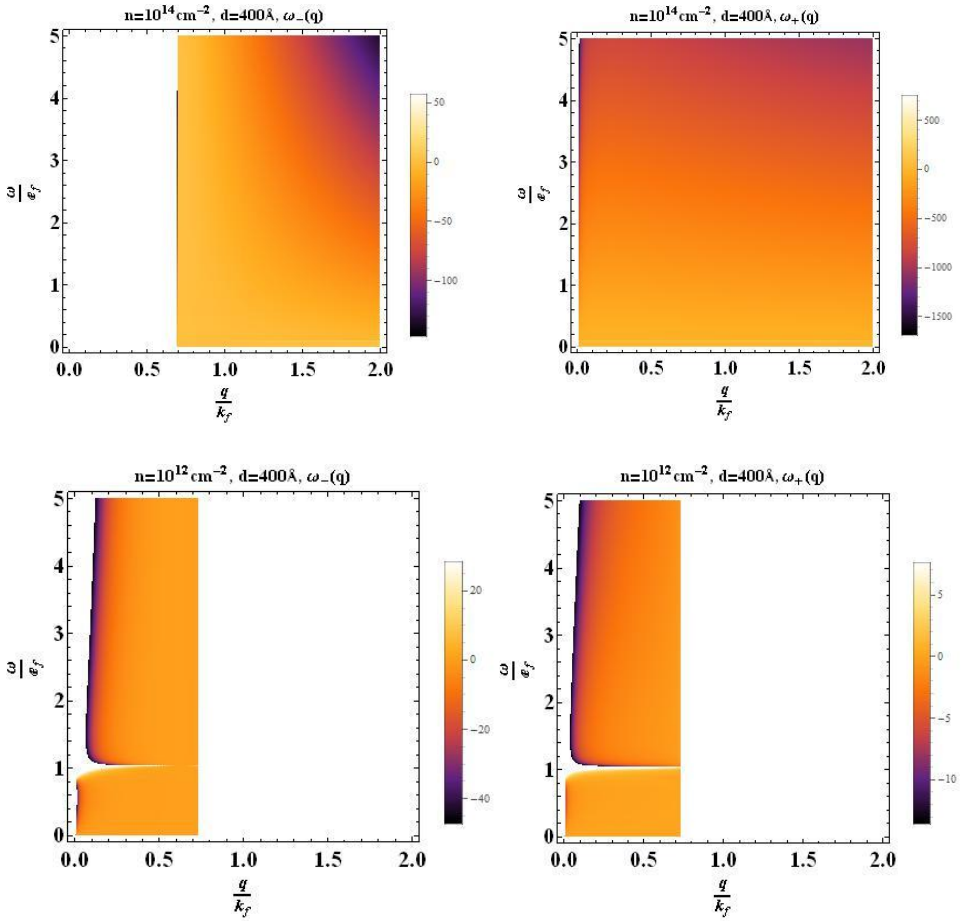

Figure 4.9 Damping in low frequency regime for GBS for different values of *n*

Using this real and imaginary part the difference in optical properties such as refractive index and attenuation due to Plasmon-phonon coupling effect can also be calculated using following formulas. The complex refractive index can be written as $N = n + i\kappa$. The frequency dependent dielectric constant is simply the square of the (complex) refractive index in a non-magnetic medium (one with a relative permeability of unity. Where $\tilde{\epsilon}$ is the complex dielectric constant with real and imaginary parts ϵ_1 and ϵ_2, and n and κ are the real and imaginary parts of the refractive index, all functions of frequency:[31]

$$\tilde{\epsilon} = \epsilon_1 + i\epsilon_2 = (n + i\,\kappa)^2 \tag{4.14}$$

Conversion between refractive index and dielectric constant is done by:

$$\epsilon_1 = n^2 - \kappa^2 \tag{4.15}$$

$$\epsilon_2 = 2n\kappa \tag{4.16}$$

$$n = \sqrt{\frac{\sqrt{{\epsilon_1}^2 + {\epsilon_2}^2} + \epsilon_1}{2}} \tag{4.17}$$

$$\kappa = \sqrt{\frac{\sqrt{{\epsilon_1}^2 + {\epsilon_2}^2} - \epsilon_1}{2}} \tag{4.18}$$

The optical properties for multilayer graphene has been reported by Yu V Bludov and group [32] The attainable values in all above reported results are similar to frequencies compatible in Near Infrared (NIR) to visible spectra (Table 4.1), and hence making it feasible to develop such high-frequency based devices. The devices working in this range are image sensors, optical fiber cables, photo detectors, modulators, opto-electronic switches etc. The electromagnetic radiations in this regime can resonate with the CPPM of GBS making it possible to realize devices working in this frequency range. Though there have been GNRs developed which can work in this same frequency regime but GBS can also be viewed as an equivalent efficient device. Plasmon-Phonon coupling mode helps to gain insight in heat capacity, thermal conductivity and various other important quantities which should be considered during device fabrication. Plasmon-Phonon coupled modes were reported for the Hetero-Superlattice [33], our results are almost similar to the results reported in the paper.

The electromagnetic spectrum is divided into various frequency regimes.

Electromagnetic Spectrum		
Name	***Wavelength λ***	***Frequency (Hz)***
γ-rays	<0.01 nm	> 30 EHz
X-Ray	0.01nm-10nm	30EHz-30PHz
Ultraviolet	10nm-380nm	30PHz-790THz
Visible	380nm-700nm	790THz-430THz
Infrared	700nm-1mm	430THz-300GHz
Microwave	1nm-1m	300GHz-300MHz
Radio	1mm-100,000km	300GHz-3Hz

Table 4.1: Frequency and wavelength regime for various sections of electromagnetic spectrum [34].

4.3.2 Energy Loss

When an external particle travels above a system it interacts with the system and loses some amount of energy to the system. This energy may or may not create plasma oscillations. The portion where plasmons are not created is known as single particle excitation regime and the portions where plasmons are created is known as collective excitation regime. These excitations are damped and decay into electron-hole pairs via loss function.

The energy loss function for a system is given as

$$Im\left(\frac{1}{\epsilon}\right) = \frac{\epsilon_2(\vec{q},\omega)}{\epsilon_1^2(\vec{q},\omega) + \epsilon_2^2(\vec{q},\omega)} \tag{4.19}$$

The energy loss function is obtained for long wavelength limit of polarization in graphene given as eq. 4.5 in low frequency regime. We have evaluated energy loss function for GBS for different values of *n* and *d.* The intensity plots have been plotted for the loss functions with the vertical bars on the right side of each figure indicates the intensity of energy loss with white color depicting the maximum loss while the black color is the zero loss function region.. For particular values of q the loss intensity is maximum in (ω, q) space. As the charge density is increased the intensity of energy loss is increased. With increase in distance between the layers (i.e. almost SLG behavior) the zero energy loss regions is less compared to more compact GBS. Thus GBS can be considered as better device making material with lesser energy loss than SLG. This low energy loss in GBS can have better technological applications as energy storage devices.

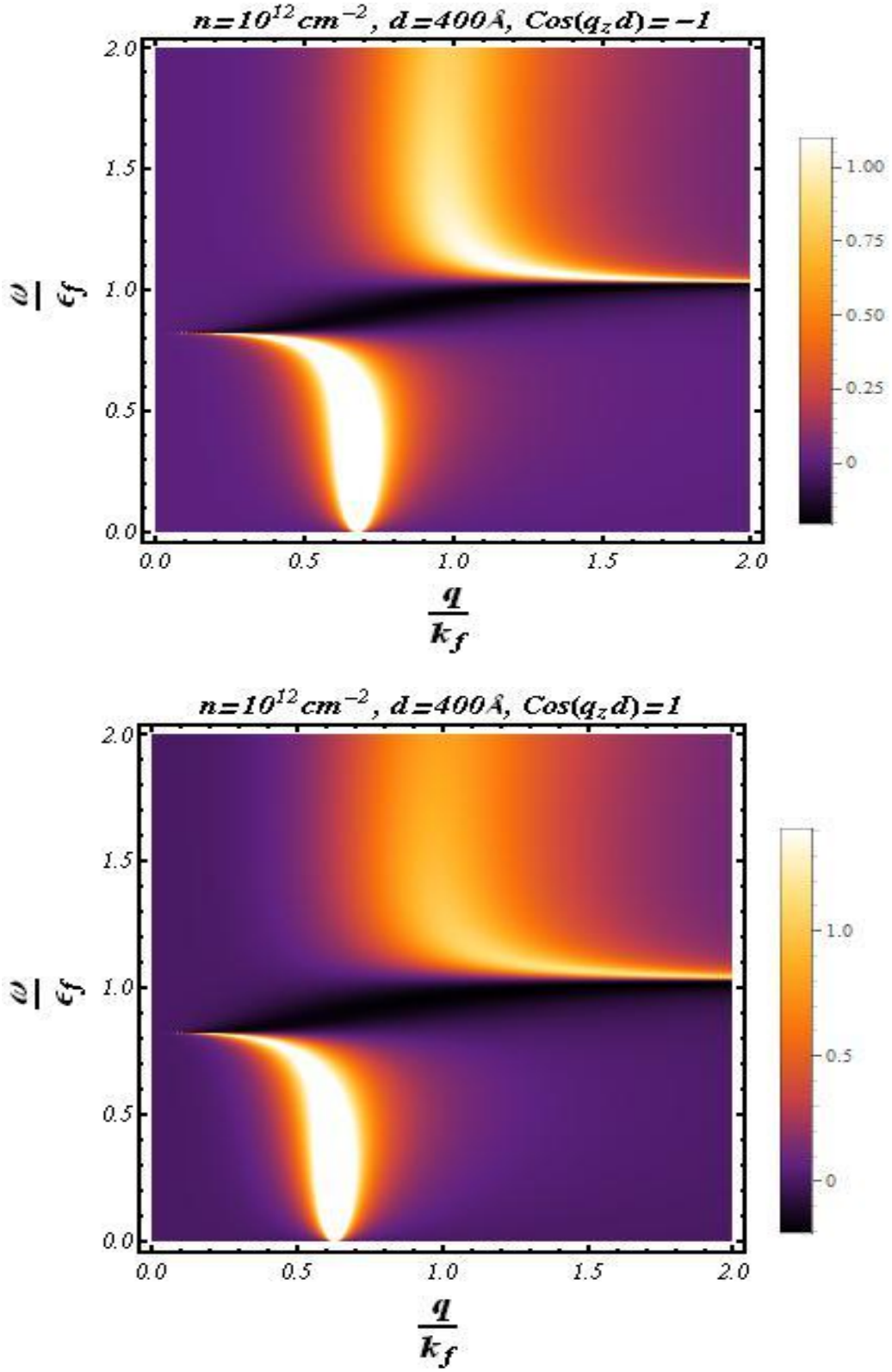

Figure 4.10 Density Plots of energy loss function of GBS plotted for n=10^{12} cm^{-2} and d=400Å for lower (*Cos* $(q_z d) = -1$) and upper boundaries (*Cos*$(q_z d)=1$).

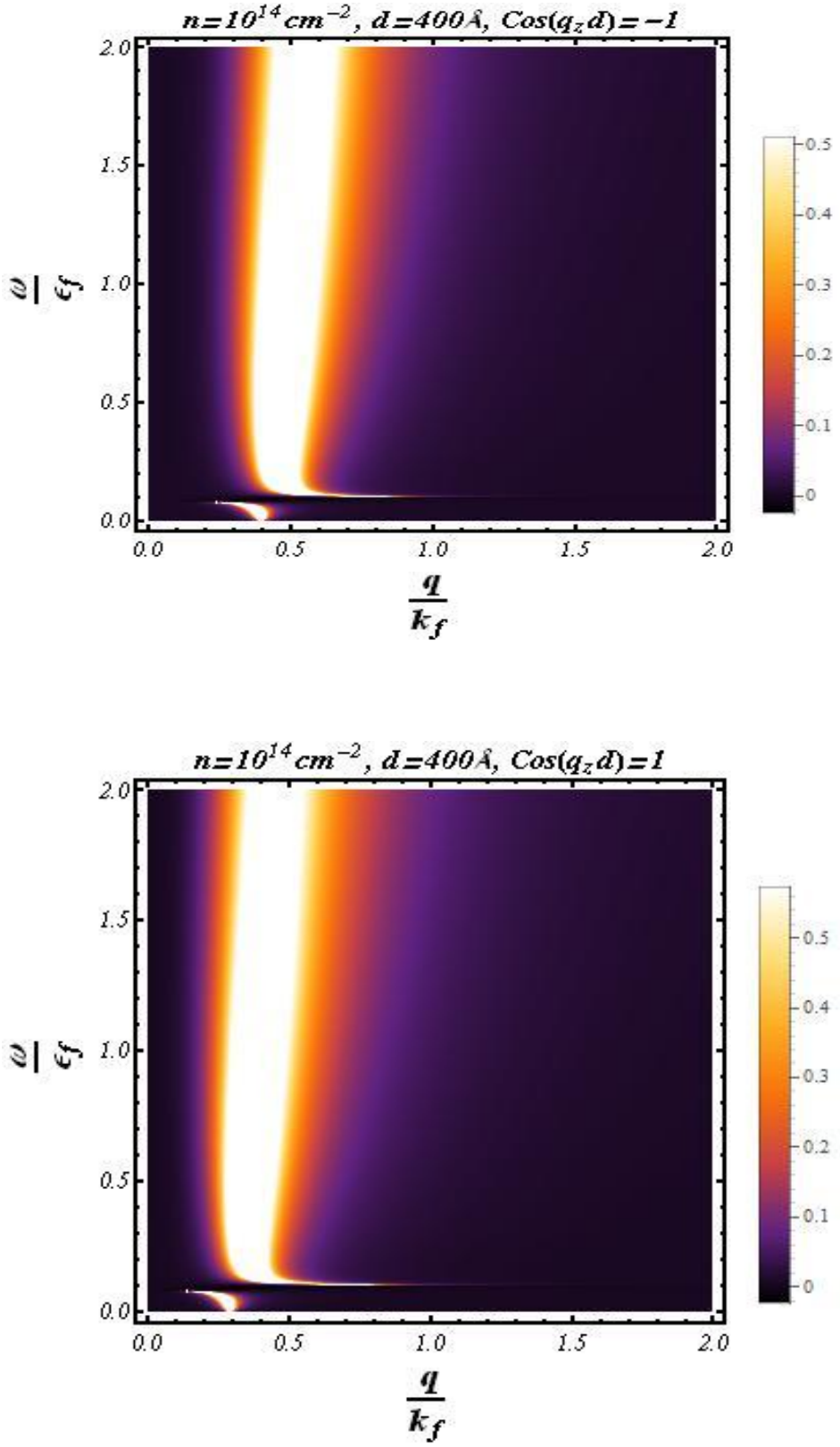

Figure 4.11 Density Plots of energy loss function of GBS plotted for n=10^{14} cm^{-2} and d=400 Angstrom for lower (*$Cos(q_z d)=-1$*) and upper boundaries (*$Cos(q_z d)=1$*).

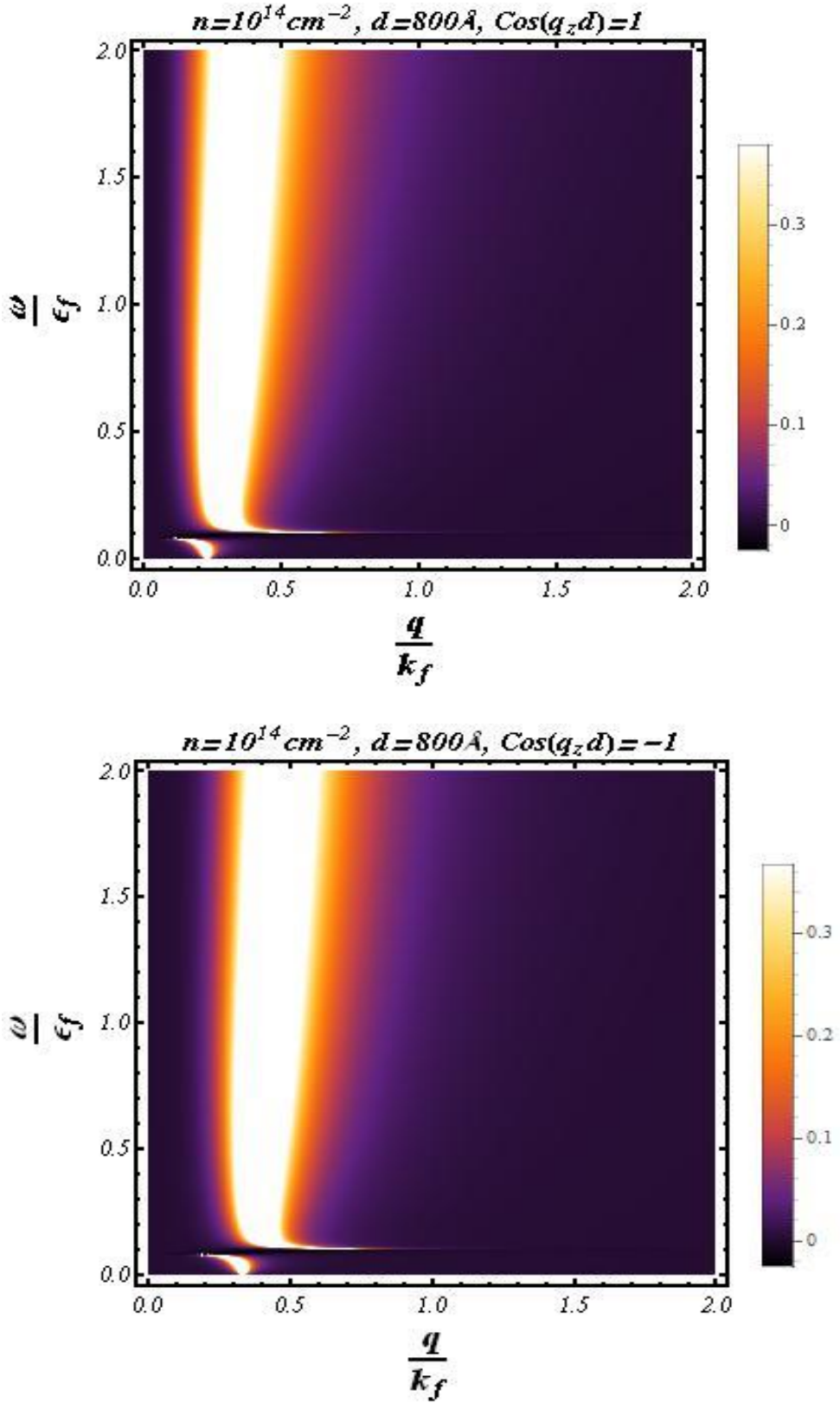

Figure 4.12 Density Plots of energy loss function of GBS plotted for $n=10^{14}$ cm^{-2} and d=800 Angstrom for lower ($Cos(q_z d)=-1$) and upper boundaries ($Cos(q_z d)=1$).

4.4 References

1. Bloss W L and Brod E M Solid state communications Vol.***43***, No. 7 pp 523-528 (1982)

2. Xiaoguang Wu, Peeters F.M. and Devreese J.T. PRB Vol**.** ***32*** No. 10 6982-6985

3. H.Altan, X.Xin, D.Matten and R.R.Alfano Appl. Phys. Lett ***89***,052110 (2006)

4. Ponomaenko and the references therein Nature ***497***, 594 (2013)

5. Frank Neubrech, Annemarie Pucci,Thomas Walter Cornelius, Shafqat Karim, Aitzol Garcia-Etxarri and Javier Aizpurua – PRL ***101***,157403 (2008)

6. A. Huber, N. Ocelic, T. Taubner, and R. Hillenbrand NANO LETTERS 2006 Vol**.** ***6***, No.4 774-778

7. H M Dong, L L Li, W Y Wang, S H Zhang, C X Zhao, W Xu Physica E ***44*** (2012) 1889–1893

8. E H Hwang, Rajdeep SenSarma, and S D Sarma Phys Rev B ***82***, 195406 (2010)

9. S D Sarma, E H Hwang Phys Rev Lett ***102***,206412 (2009)

10. Yuan Shengjun, R Roldan, and M I Katsnelson. Phys Rev ***B 84***, 035439 (2011)

11. N J M Horing Phil. Trans. R. soc. A 2010 ***368***, 5525-5556

12. J J Zhu, S M Badalyan, and F M Peeters Phys. Rev**.** ***B 87***, 085401 (2013)

13. Freitag *et.al.* arXiv 1306.0593v1

14. Yan Hugen *et.al.* arXiv 1209.1984v1

15. J. Luxmoore, C. H. Gan, P. Q. Liu, F. Valmorra, P. Li, J. Faist, and G. R. Nash - arXiv preprint arXiv:1405.7607 (2014)

16. Xiaolong Zhu, Weihua Wang, Wei Yan, Martin B. Larsen,, Peter Bøggild, Thomas Garm Pedersen, Sanshui Xiao, Jian Zi,⊥ and N. Asger Mortensen

17. A.Politano, V Formoso and G Chiarello J.Phys : Cond. Matter ***25*** 345303 (2013)

18. Z.L. Miskovic - Gran Sasso National lab GraphITA 15-18 May 2011

19. Tony Low and Phaedon Avouris Vol ***8*** No.2 1086-1101 (2014)

20. Xiaoguang Luo, Teng Qiu, Weibing Lu, Zhenhua Ni Vol.***74***, Issue 11, Nov. 2013, Pages 351-376

21. S. Katayama, K. Murase and H.Kawamura – Solid State Communications, Vol.***16***, pp. 945-948, (1975)

22. Yu Liu, R F Wills Phys. Rev. ***B 81,*** 081406(R) (2010)

23. Yuxiang Ni, Yann Chalopin and Sebastian Volz Appl. Phys. Lett. ***103***, 141905 (2013)

24. J.A.Briones-Torres, J.Madrigal-Melchor, J.C.Martinez-Orozco, I.Rodriguez-Vargas Superlattices and Microstructures ***73*** (2014) 98-112

25. Jain Jainendra and Allen Phys. Rev. Lett. ***54***, Number 22 2437-2440 (1985)

26. A.C. Sharma and A.K. Sood J.Phys. cond. matter ***6*** (1994) 1553-1562

27. E H Hwang and S D Sarma Phys. Rev***. B 75***, 205418 (2007)

28. A.L. Fetter and J.D. Walecka ***Quantum Theory of Many-Particle systems***, Dover Publications

29. G D Mahan, ***Many Particle Physics*** IInd Ed. (Plenum, newYork, 1990)

30. B.K.Ridley ***Electrons and Phonons in semiconductor multilayers***

31. M. Dressel and Gruner George Electrodynamics of Solids - ***Optical properties of Electrons in Matter***, Cambridge University Press

32. Yu V Bludov, N M R Peres and M I Vasilevskiy J. Opt***. 15*** (2013) [114004]
33. Falkovsky JETP Letters, Vol. ***82***, No. 2, 2005, pp. 96–100(2005)

34. Haynes, William M., ed. (2011). CRC ***Handbook of Chemistry and Physics*** (92nd ed. ed.). CRC Press. p. 10.233. ISBN 1-4398-5511-0